

# Decoupling transition of two coherent vortex arrays within the surface superconductivity state

Alexey V. Pan<sup>1,2\*</sup> and Pablo Esquinazi<sup>1</sup>

<sup>1</sup>Abteilung Supraleitung und Magnetismus, Institut für Experimentelle Physik II,  
Universität Leipzig, Linnèstraße 5, D-04103 Leipzig, Germany

<sup>2</sup>Institute for Superconducting and Electronic Materials, University of Wollongong,  
Northfields Avenue, Wollongong, NSW 2522, Australia

(Dated: May 9, 2003, Revised: July 21, 2004)

In magnetic fields applied within the angular range of the surface superconductivity state a magnetically anisotropic layered medium is created in structurally isotropic, sufficiently thick niobium films. Surface (Kulik) vortices residing in the superconducting sheaths on both main film surfaces in tilted fields are shown to undergo a decoupling transition from a coherent to an independent behavior, similar to the behavior observed for Giaever transformer. At the transition a feature in pinning properties is measured, which implies different pinning for the lattice of surface vortices coherently coupled through the normal layer and for two decoupled vortex arrays in the superconducting surface sheaths.

PACS numbers: 74.25.Op, 74.25.Qt, 74.25.Ha, 74.78Db

## I. INTRODUCTION

The existence of vortices and vortex states within the surface superconductivity (SC) state has been discussed since the discovery<sup>1</sup> of this phenomenon within the applied magnetic field range  $B_{c2} \leq B_a \leq B_{c3}$  ( $B_{c2}$  and  $B_{c3}$  are the second and surface superconductivity critical fields). The existence of Abrikosov vortices<sup>2</sup>, Abrikosov-like state<sup>3,4</sup>, giant (multi-quantum) vortex state<sup>5,6,7</sup>, and Kulik (surface) vortices<sup>8,9,10</sup> above  $B_{c2}$  were suggested depending on sample size and shape and applied field orientation. In this work, we mainly deal with the magnetic behavior governed by *surface vortices* in the superconducting surface sheath. The structure of a surface vortex, to a large extent, reproduces the structure of an Abrikosov vortex with the length equal to the thickness of the superconducting layer (surface sheath). Fink and Kessinger showed<sup>11</sup> that the thickness of this sheath  $d_{sc} \simeq 1.6\xi(T)$  at  $B_a \simeq B_{c2}$  and approaches  $\xi$  at  $B_a = B_{c3}$  for a superconductor with  $\kappa = 10$  ( $\kappa = \lambda/\xi$  is the Ginzburg-Landau parameter,  $\xi$  and  $\lambda$  are the coherence length and magnetic field penetration depth). In the case of a relatively thin superconductor, as the films investigated in this work, the superconducting surface sheaths on the main film surfaces are separated by a normal layer

$$d_n \simeq d_p - 3.2\xi(T) \quad (1)$$

with  $d_p$  being the film thickness.

For a certain magnetic field range applied at an angle ( $\theta$ ) to the surfaces, two independent flux-line lattices (FLLs) can be formed in thin films and layered systems.<sup>4,8,9,10,12,13,14,15,16,17</sup> This co-existence is possible due to strong structural or magnetic anisotropy and to the two components of the applied field.<sup>8,12</sup> In this case, the out-of-plane field component ( $B_{a\perp}$ ) would be responsible for the out-of-plane (perpendicular) FLL and the in-plane (parallel) component ( $B_{a\parallel}$ ) for the in-plane

vortex lattice. The co-existence of two FLLs has experimentally been shown for structurally isotropic films similar to those investigated in this work<sup>4,14,15,16</sup>. Therefore, we will hereafter assume that in the films investigated two co-existing FLLs, perpendicular and parallel to the main film surface, are present at fields tilted with respect to the surface. Fig. 1(a) schematically shows the two-FLLs structure.

We further assume that at  $B_a > B_{c2}$  and over the angular range of  $|\theta| < 40^\circ$ , which is the range over which the surface SC state can be measured:<sup>3,4</sup> (i) the parallel FLL in thick films  $d_p \gg \xi$  transforms into a giant vortex above  $B_{c2}$ .<sup>6,7,15,17</sup> This is a reasonable assumption because the surface SC state, just like the in-plane Abrikosov vortex rows, forms due to the  $B_{a\parallel}$  component. The shielding super-currents of the giant vortex flow within the surface sheath. (ii) The perpendicular FLL forms two arrays of quasi-2D surface vortices residing in the superconducting sheaths on both main surfaces of the films<sup>8</sup> (Fig. 1(b)). The co-existence of the giant vortex and the surface vortices was discussed in Refs. 9,10. It was also shown that Kulik vortices can form triangular or square lattice, depending on the applied field and its orientation  $\theta$ .<sup>8</sup>

Neither theoretical nor experimental work has been published, which shows any kind of interaction between the two surface vortex arrays on the opposite surfaces of a thin flat sample in the surface SC state. We expect that the arrays can behave either coherently or independently, depending on  $d_n$ ,  $d_{sc}$ ,  $B_a$  and  $\theta$ . These parameters can affect the coupling force between the vortices as it was shown for the case of two magnetically coupled superconducting films (superconducting Giaever transformer<sup>18</sup>) in fields  $B_a < B_{c2}$ .<sup>19,20</sup> At the transition between the coherent and independent regimes a *small pinning change* would be expected. Therefore, one needs a technique sensitive to such small changes in fields applied *nearly parallel* to the film surface. Such fields are necessary to

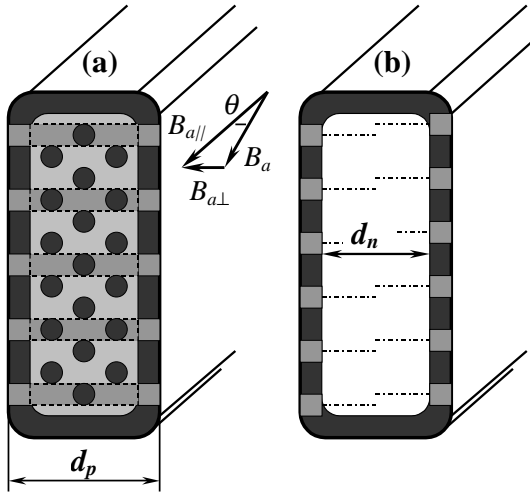


FIG. 1: The vortex arrangements are schematically shown for the film cross-section in a field  $B_a$  applied at an angle  $\theta$  to the main film surfaces (a) below  $B_{c2}$ , and (b) above  $B_{c2}$  after the decoupling transition. The black layer near the circumference of the film denotes the surface SC sheath with the light gray surface vortices in it. The black circles in (a) imply in-plane Abrikosov vortex rows<sup>2,4</sup> parallel to the surfaces. The dark grey stripes perpendicular to the surfaces show the out-of-plane Abrikosov vortices. Although it is not clear on the picture but it is assumed that vortex lines of both Abrikosov lattices in (a) do not cross one another.

enable the surface SC state. In this work, we describe results of mechano-magnetic experiments on niobium (Nb) films of different thicknesses and provide experimental evidence for the decoupling transition of the surface vortices within the surface SC state.

## II. EXPERIMENTAL DETAILS

The experimental technique employed in this work is based on mechanical oscillations of a superconductor attached to a Vibrating Reed (VR) in an external magnetic field (for a review see Ref. 21 and references therein). The experimental VR setup employed in this work can be found in Ref. 4. This technique is very sensitive to magnetic properties of the superconductor, in particular to the pinning of vortices, in fields parallel to its largest surface ( $\theta = 0^\circ$ ). The physical reason for this sensitivity is that the very small field component  $\sim B_a \varphi$  perpendicular to the applied field, arising when the superconductor is tilted by a very small angle (typically  $\varphi < 10^{-5}$  degrees), is shielded by superconducting currents (generally defined by the pinning of vortices). The shielding currents cause the external field to curve around the tilted superconductor. This field distortion leads to an additional line tension (stiffness) in the system, which

is proportional to the increase of the length of the field lines near the edge of the tilted superconductor. As a result, the resonance frequency ( $\omega$ ) of the VR with the attached superconducting sample increases with field. If the shielding supercurrents become smaller, for example in the vicinity of the upper critical field or the critical temperature (in general due to a pinning reduction), the resonance frequency decreases. The damping ( $\Gamma$ ) of the oscillator, which is measured simultaneously with the resonance frequency, is proportional to the corresponding energy dissipation occurring in the oscillator (reed plus superconducting sample) due to vortex movement and the internal friction of the reed material. The peak in the damping, usually measured as a function of field or temperature, corresponds to the vortex depinning line.<sup>22</sup> However, in the case of the surface superconductivity (the so-called giant vortex state) the peak can have a different origin related to the shielding/pinning properties of the giant vortex (see, for example, Ref. 6 and references therein).

In the case of a *thin* conventional superconductor, such as Nb-film, the behavior of the VR as a function of temperature and field is, to a large extent, governed by the magnetic properties of the surface of the superconductor. Therefore, the unique properties of the VR technique should allow us to detect changes in the behavior of the surface vortex arrays, whose pinning can influence the shielding property. Accordingly, the resonance frequency change  $\omega^2(B_a) - \omega^2(0)$  and the damping  $\Gamma(B_a)$  measured in the experiment are respectively expected to provide information on surface vortex pinning and energy dissipation produced by vortex movement.

The increase in the resonance frequency vanishes as soon as vortex pinning and the shielding become negligible. Thus, we can measure not only  $B_{c2}$  at  $\theta \rightarrow 90^\circ$  and  $B_{c3}$  at  $\theta \rightarrow 0^\circ$ , but also the angular dependence of the upper critical field ( $B_{uc}(\theta)$ ).<sup>3,4,15</sup> Naturally, we define  $B_{uc}(\theta = 0^\circ) \equiv B_{c3}$  and  $B_{uc}(\theta = 90^\circ) \equiv B_{c2}$ .

Another important feature of our experimental setup is the high angular resolution of the rotation system.<sup>4</sup> As a consequence, the angle  $\theta$  of the field with respect to the main film surface was defined with an accuracy of  $\pm 0.01^\circ$  in the vicinity of  $0^\circ$  and of  $\pm 0.5^\circ$  at  $\theta \gtrsim 3^\circ$ . At  $\theta \gg 0^\circ$ , the angular resolution is smaller for these experiments due to a small  $\Delta^2 B_{cu}/(\Delta\theta)^2$  at  $\theta \neq 0^\circ$  (see Fig. 5 in Ref. 4). The accuracy near  $0^\circ$  is limited by the sensitivity of the Si-oscillator onto which the superconducting sample is attached. This Si-oscillator has a quality factor  $Q \sim 10^6$  at the temperatures of the measurements.

Nb-films of different thicknesses  $d_p \simeq 120$  nm (Nb120), 400 nm (Nb400), and 1200 nm (Nb1200) were investigated in this work. The polycrystalline films were sputtered onto an oxidized silicon wafer at room temperature.<sup>23</sup> Superconducting properties of these films were characterized in earlier works.<sup>4,14,15</sup> The coherence length at zero temperature  $\xi(0)$  for all the measured samples was estimated to be  $\sim 12.5$  nm ( $\xi(T = 5\text{ K}) \simeq 19$  nm). We estimate a Ginzburg-Landau parameter

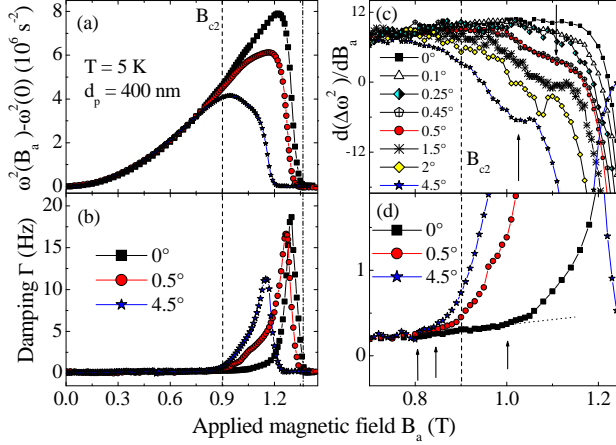


FIG. 2: (a) The resonance frequency change  $\Delta\omega^2 \equiv \omega^2(B_a) - \omega^2(0)$ , (b) the corresponding damping, (c) the first derivative of  $\Delta\omega^2$  on  $B_a$  with the arrows denoting the minima ( $B_m$ ), and (d) the enlargement of the damping onset at  $B_{\text{onset}}$  which is marked by the arrows for the Nb400-film. The dashed and dashed-dotted lines mark  $B_{c2}$  and  $B_{c3}$ , respectively.

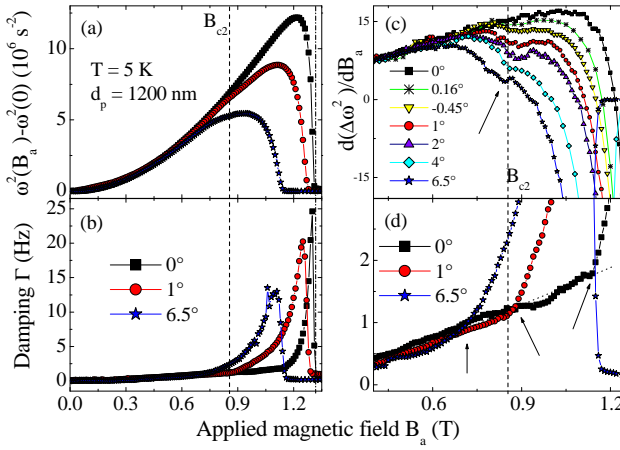


FIG. 3: The same as in Fig. 2 for the Nb1200-film.

$\lambda/\xi \sim 10$  for the three films.<sup>4</sup>

### III. EXPERIMENTAL RESULTS

Figures 2 and 3 show the measured resonance frequency change  $\omega^2(B_a) - \omega^2(0)$  (a) and the VR damping  $\Gamma(B_a)$  (b) as a function of applied field at different angles  $\theta$  and at fixed temperatures for the Nb400 and Nb1200-films, respectively. The key-feature in these figures is the appearance of an unusual non-monotonic behavior at angles  $\theta \geq \theta_m^{\text{on}}$ , which is best seen as a minimum at a field we define as  $B_m$  in the first derivative of the resonance frequency (Figs. 2(c) and 3(c)). This “critical” angle  $\theta_m^{\text{on}}$  is  $\simeq 0.45^\circ$  and  $0.16^\circ$  for the Nb400- and Nb1200-films, respectively.  $B_m(\theta)$  for both films is shown

in Fig. 4(a). The angular range of the non-monotonic behavior ( $\theta_m^{\text{on}} \leq \theta_m < 20^\circ$ ) is within the range of the surface SC existence.<sup>4,15</sup> In principle, one would tend to observe the position of the minima ( $B_m$ ) at  $B_{c2}$ . In this case, the minima would naturally indicate a change in the shielding property when the bulk superconductivity collapses and only surface superconductivity persists. However, the minima do not coincide with the experimentally measured  $B_{c2}$  (marked by the dashed lines in Figs. 2, 3, and 4). Instead, the  $B_m$ -behavior is more complex being angular dependent. We argue below that this behavior can be explained as *decoupling of the coherent arrays of the surface vortices*, which undergo a decoupling transition from coherent behavior at  $B_a < B_m$  to independent behavior at  $B_a > B_m$ . This transition is promoted by the magnetically anisotropic medium created in the films in fields within  $B_{c2} \leq B_a < B_{c3}$  applied nearly parallel to the surface. Taking into account the thickness of the films, the coupling between the coherent surface vortex pairs is of *magnetic* nature.

## IV. DISCUSSION

### A. Angle dependence of $B_m$

At  $\theta < \theta_m^{\text{on}}$ ,  $B_{a\perp}$  is too small to induce a large density of surface vortices in the surface sheaths. This is likely to imply that the magnetic behavior in this angular range is overwhelmingly governed by the giant vortex surface shielding current. Therefore, the VR signal is not sensitive enough to reveal a possible decoupling transition for only a few surface vortices up to  $B_{cu}$ . As  $\theta$  becomes larger (Fig. 4(a)),  $B_{a\perp}$  increases and more *coupled* surface vortices are created. These vortices start interacting within each sheath at a characteristic crossover field given by<sup>20</sup>

$$B_{cr} = \frac{2\Phi_0}{\sqrt{3}(a_0^{cr})^2}, \quad (2)$$

where  $\Phi_0$  is the flux quantum and  $a_0^{cr}$  is the intervortex distance at the crossover. As soon as intervortex interaction between surface vortices within one sheath becomes stronger than the coupling force, the decoupling between the coherent pairs of surface vortices takes place, forming two independent arrays of (2D-like) vortex lattices, one in each surface sheath. The magnetic coupling of the surface vortices is weak due to the relatively large distance  $d_n$ . Thus, relatively weak in-plane vortex-vortex interaction should be enough to decouple the coherent behavior. A sufficiently strong intervortex interaction for a decoupling would occur at an intervortex distance  $a_0^{cr} \sim 2\lambda(T)$ . If we assume that the intervortex spacing for the triangular surface vortex lattice is<sup>8</sup>

$$a_0 \simeq (2\Phi_0/\sqrt{3}B_a \sin \theta)^{0.5}, \quad (3)$$

one finds that at  $\theta_m^{\text{on}}$ ,  $a_0 \simeq 0.5 \mu\text{m}$  for the Nb400-film and  $a_0 \simeq 1 \mu\text{m}$  for the Nb1200-film. Thus, the intervortex spacing is of the order of  $2\lambda(T = 5\text{K}) \sim 0.38 \mu\text{m}$  at  $\theta_m^{\text{on}}$ .

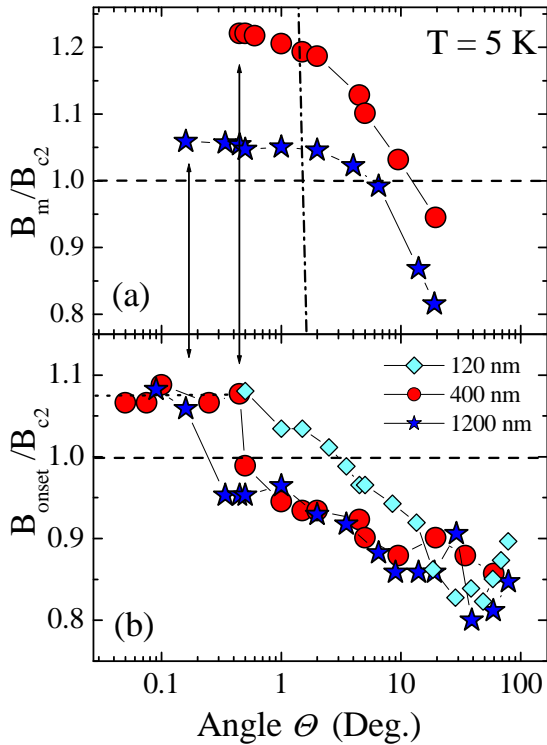


FIG. 4: (a) Normalized field  $B_m$  at which minima are observed in the resonance frequency change, and (b) damping onset as a function of angle. The arrows mark  $\theta_m^{on}$  in (a) coinciding with the step-like feature in (b) for the Nb400- and Nb1200-films. The dash-dotted, nearly vertical line in (a) shows  $B_{cr}(\theta)$  obtained from Eq. (3) assuming a fixed value for the intervortex distance  $a_0 = a_0^{cr} = 2\lambda(5 \text{ K}) = 380 \text{ nm}$ . The dotted line in (b) shows the plateau at small angles and an additional experimental point measured at  $\theta = 0^\circ$  for the films, which cannot be shown in the logarithmic scale.

Let us assume that the decoupling transition occurs when the perpendicular component of the applied field  $B_{a\perp} \equiv B_a \sin \theta$  is equal to  $B_{cr}$ . Then, the dash-dotted line in Fig. 4(a) shows  $B_{cr}(\theta) \propto (a_0^2 \sin \theta)^{-1}$  expected from Eq. (3) with the fixed  $a_0 = a_0^{cr} = 2\lambda(T = 5 \text{ K}) = 380 \text{ nm}$  for the Nb1200- and Nb400-films. As can be seen, Eq. (3) with the fixed  $a_0$  does not describe the  $B_m(\theta)$  behavior over the entire decoupling line except at the angle  $\sim 1.5^\circ$  at which the calculated curve crosses the corresponding experimental  $B_m$ -lines. The disagreement between the experimental curves and Eq. (3) should actually be expected. Indeed, in the case of Eq. (3) only one parameter –  $a_0(B_{a\perp})$  – affecting the decoupling, changes with field (or angle). Whereas in our case there are at least four variables affecting the coupling:  $a_0(B_{a\perp})$ ,  $d_{sc}(B_{a\parallel})$ ,  $d_n(d_{sc})$  and surface vortex pinning. The behavior of the  $B_m(\theta)$  curves in Fig. 4(a) can be explained by four major factors, which influence the above mentioned variables: (i) the nature of the decoupling

which occurs within the surface SC state and with an enormously large interlayer spacing  $d_n$  and small  $d_{sc}$ , (ii) surface roughness of the measured films, (iii) surface vortex pinning which is not accounted for in Eq. (3), and (iv) angular dependence of the upper critical field  $B_{cu}$ .

The *first* factor responsible for the  $B_m$  behavior below the crossing point is particularly well described on the example of the thicker film (Nb1200) with *much weaker coupling* (due to the larger  $d_n$ ) than that in the Nb400-film. For the Nb1200-film the  $\theta$ -independent plateau is observed for  $B_m$  at  $\theta \leq 2^\circ$ . In this range the decoupling is driven by the reduction of  $d_{sc}$  above  $B_{c2}$  with increasing  $B_a$ .<sup>11</sup> The smaller  $d_{sc}$  (the larger  $d_n$ ) leads to a reduction of the coupling and pinning for both surface vortices of all coupled pairs. As soon as the decoupling threshold is reached, the surface vortices from each pair are likely to be dragged apart by shielding currents incoherently oscillating on opposite surface sheaths. As  $\theta$  approaches the crossing point at  $\sim B_{cr}$ ,  $B_m$  starts to curve downwards being also affected by intervortex interactions. A similar, but stronger effect experiences the thinner film (Fig. 4(a)). The stronger angular dependence below the crossing point is likely observed because the decoupling threshold is higher than for the thicker film. Hence, to reach the decoupling higher fields have to be applied (Fig. 4(a)), which result in larger surface vortex populations and, consequently, in stronger intervortex interactions.

The *second* factor can have some influence in the vicinity of the crossing point. The values of  $a_0$ , calculated for “ideal” film surfaces, are likely to be underestimated due to the surface roughness present in real films.<sup>24</sup> The surface roughness model implies that even if  $\theta = 0^\circ$ , the flux would intercept some localized areas of the rough surface. Thus, the rougher the surface, the more surface vortices are expected to populate the sheaths in applied fields nearly parallel to the surface. The Nb1200-film was found to have a larger value of the root mean square surface roughness (6.6 nm) than the Nb400-film (5.3 nm).<sup>15</sup> This result can contribute to the fact that the decoupling has been observed starting from a smaller  $\theta_m^{on}$  for the Nb1200-film than for the thinner film. Apparently, at larger angles the surface roughness factor becomes less significant.

The *third* factor is responsible for the disagreement at larger angles. The pinning experienced by the surface vortices<sup>10,24,25</sup>, which we neglected to a large extent in the above consideration, is likely to modify significantly Eq. (3) derived by assuming pinning-free environment.<sup>8</sup>

The *fourth* factor can also influence  $B_m$  in particular at larger angles, since, for example,  $B_{cu}$  at  $5^\circ$  is about 10% smaller than  $B_{c3}$ .<sup>4,15</sup> This can affect the thickness of the surface sheath  $d_{sc}$ , pinning and shielding properties, and, therefore, the decoupling.

In Fig. 4(a) one sees that increasing  $\theta$ ,  $B_m$  approaches  $B_{c2}$ . It may seem surprising that the feature attributed to the decoupling in the surface SC state still exists below  $B_{c2}$ . However, it was shown in a number of

theoretical<sup>7,26,27</sup> and experimental works<sup>15,17,28</sup> that a giant vortex state within a superconducting surface sheath can be nucleated at sufficiently high fields below  $B_{c2}$ . In this case, the magnetic anisotropy (the layered structure) of the surface SC state can also be preserved below  $B_{c2}$ . In addition, the superconducting order parameter within the  $d_n$ -layer is substantially reduced due to a large number of densely packed in-plane Abrikosov vortices.<sup>27</sup> In this case the magnetic anisotropy (layered structure) is effectively maintained below  $B_{c2}$ . We stress that the decoupling is observed only within the angular range of the surface SC state existence ( $0 \leq \theta \leq 40^\circ$ )<sup>4,15</sup> defined as  $B_{cu} > B_{c2}$ . Therefore, the decoupling appears to be a realistic scenario below  $B_{c2}$ , as well.

Summarizing, the decoupling behavior in Fig. 4 can be described as follows. At  $\theta < \theta_m^{on}$ , the giant vortex shielding overwhelmingly dominates, so that the possible decoupling of only very few surface vortices cannot be detected by the VR technique: neither the measured resonance frequency change nor damping show an unusual behavior up to the vicinity of  $B_{c3}$  as if there were no transition at  $B_{c2}$ . At  $\theta \geq \theta_m^{on}$  the decoupling occurs at  $B_m(\theta)$ . At fields below the decoupling pinning and shielding properties behave in a usual way as described for the VR technique.<sup>4,21,22</sup> As the field further increases the coupling force between the sufficiently large amount of surface vortex pairs becomes too small to prevent the decoupling. The decoupling is likely driven by two different mechanisms below and above the crossing point: (i) Below the crossing point, as the coupling forces become too small due to the  $d_{sc}$  reduction with increasing field, the independent surface vortices become more mobile due to incoherent oscillation of the shielding currents on the opposite film's surfaces. As the result, the shielding properties slightly weakens (resonance frequency), and the dissipation notably onsets (damping). However, the mobility of the vortices is expected to be incomplete due to the arising pinning of individual surface vortices. (ii) Above the crossing point, this scenario is further complicated by an additional parameter: intervortex interaction, which assists in the decoupling process. In this case, the mobility of the vortices would be restricted by a collective process which arises from interplay between vortex-vortex interaction and pinning of the surface vortices.

In both cases, the shielding would be slightly weakened at the decoupling and partially regained after pinning independent 2D-like surface vortex arrays in the superconducting surface sheaths. Experimentally, this behavior has produced the observed minima in the first derivative of the resonant frequency change (Figs. 2(c) and 3(c)) and the apparent enhancement of the damping at  $B_{\text{onset}}$  (see the arrows in Figs. 2(d) and 3(d)). Note that in Fig. 4(b), the  $B_{\text{onset}}(\theta)$  dependences for the Nb400 and Nb1200-films show step-like features at  $\theta_m^{on}$ . These steps coincide precisely with the appearance of  $B_m$  in the resonance frequency change for both films.

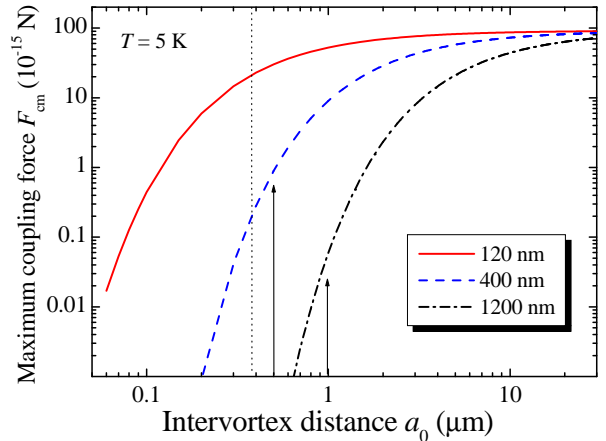


FIG. 5: The maximum coupling force ( $F_{cm}$ ) between two surface vortex arrays on the opposite film surfaces as a function of the intervortex distance ( $a_0(B_{a\perp})$ ) between the surface vortices (Eq. 4). The dotted line indicates  $a_0 = 2\lambda = 0.38 \mu\text{m}$  at  $T = 5 \text{ K}$ .

## B. Coupling force

For simplicity, assuming that the thickness of the superconducting surface layer  $d_{sc} \simeq 1.6\xi$  (in fact,  $d_{sc}(B_{a\perp})^{11}$ ), the maximum coupling force ( $F_{cm}$ ) at high-flux density regime ( $B > B_{cr}$ ) is given by<sup>20</sup>

$$F_{cm} = \frac{3\Phi_0^2 a_0^2}{32\pi^4 \mu_0 \lambda^4} \left[ 1 - \exp\left(-\frac{2\pi}{a_0} d_{sc}\right) \right]^2 \exp\left(-\frac{2\pi}{a_0} d_n\right), \quad (4)$$

provided that  $d_{sc}/\lambda \ll 1$ ,  $d_n \ll \lambda^2/d_{sc}$ , and  $\xi \ll a_0/(2\pi) \ll \lambda$ , where  $\mu_0$  is the permeability of free space. However, we should note that some of the actual conditions for the Nb1200-film at  $T = 5 \text{ K}$  are slightly softer than the given above:  $d_n < \lambda^2/d_{sc}$  and  $a_0/(2\pi) < \lambda$ . We believe that it should be acceptable for our estimate, especially taking into account that the main condition of thin superconducting layers  $d_{sc}/\lambda \ll 1$  is fulfilled.<sup>20</sup> In addition, we also note that  $\lambda$  becomes larger and  $d_{sc}$  smaller with increasing field, reinforcing the applicability of the corresponding inequalities.

In Fig. 5,  $F_{cm}$  as a function of  $a_0(B_{a\perp})$  is shown for all the films. At the decoupling crossover ( $\theta_m^{on}$ ) indicated by the arrows,  $F_{cm} \simeq 8.9 \times 10^{-16} \text{ N}$  and  $5.9 \times 10^{-17} \text{ N}$  for the Nb400- and Nb1200-films, respectively.

Taking into account the trend for thinner films to produce the decoupling onset ( $\theta_m^{on}$ ) at larger angles and stronger magnetic fields (Fig. 4(a)), the expected decoupling onset for the Nb120-film would be at or slightly below  $a_0 \simeq 2\lambda$  (the dotted line in Fig. 5). In this region,  $F_{cm}$  is *much larger* for the Nb120-film than that for the thicker films. Importantly, it is nearly within the region where  $F_{cm}$  is nearly independent on  $B$ . There-

fore, to observe the decoupling transition a much larger  $B_{a\perp}$  (smaller  $a_0$ ), implying larger  $\theta$ , should be applied in order to reduce  $F_{cm}$  and to increase the intervortex interaction. However, a minimum in the resonance frequency corresponding to the decoupling was not observed for this film, nor the step-like feature in the behavior of  $B_{\text{onset}}(\theta)$  (Fig. 4(b)). Instead,  $B_{\text{onset}}(\theta)/B_{c2}$  is clearly larger than for the thicker films. This behavior indicates stronger shielding and pinning, which remain unaffected by the decoupling but affected by the critical field dependence  $B_{cu}(\theta)$  only.

## V. CONCLUSION

In summary, from VR experiments on thin Nb films we have obtained evidence indicating that for sufficiently thick films the surface vortices in the surface SC state undergo a decoupling transition. At small fields/angles the aligned vortices are coupled through the normal layer  $d_n$  exhibiting a coherent 3D-like vortex lattice behav-

ior. At larger fields/angles the surface vortices decouple forming two independent vortex arrays (2D-like behavior) in the superconducting surface sheaths. In films with  $d_p \lesssim \lambda$ , the coupling between the aligned surface vortices appears to be too strong so that the experimental observation is not possible with the VR technique. By comparison, we note that the loss of the 3D coherence in a lattice of aligned pancake vortices in layered high-temperature superconductors was explained in terms of a melting phase transition from the 3D vortex pinning state to the regime of independently pinned 2D vortex lattices for Josephson<sup>13</sup> and magnetic<sup>29</sup> couplings between the superconducting layers.

## Acknowledgments

We would like to thank C. Assmann (PTB, Berlin) for providing us the films and R. Höhne for the support during the measurements.

\* Electronic address: pan@uow.edu.au

- <sup>1</sup> D. Saint-James and P. G. de Gennes, Phys. Lett., **7**, 306 (1963); C. F. Hempsted and Y. B. Kim, Phys. Rev. Lett. **12**, 145 (1964); W. J. Tomash and A. S. Joseph, Phys. Rev. Lett. **12**, 148 (1964).
- <sup>2</sup> I. O. Kulik, Zh. Eksp. Teor. Fiz. **52** (Rus.), 1632 (1967) [JETP **25**, 1085 (1967)].
- <sup>3</sup> M. Ziese, P. Esquinazi, S. Knappe, and H. Koch, J. Low Temp. Phys. **103**, 71 (1996).
- <sup>4</sup> A. V. Pan, M. Ziese, R. Höhne, P. Esquinazi, S. Knappe, and H. Koch, Physica C **301**, 72 (1998).
- <sup>5</sup> P. R. Doidge and K. Sik-Hung, Phys. Lett. **12**, 82 (1964).
- <sup>6</sup> R. W. Rollins and J. Silox, Phys. Rev. **155**, 404 (1967).
- <sup>7</sup> H. J. Fink, Phys. Rev. Lett. **16**, 447 (1966); M. Ghinovker, I. Shapiro, and B. Ya. Shapiro, Phys. Rev. B **59**, 9514 (1999); V. Bruyndoncx, J. G. Rodrigo, T. Puig, L. Van Look, V. V. Moshchalkov, and R. Jonckheere, Phys. Rev. B **60**, 4285 (1999).
- <sup>8</sup> I. O. Kulik, Zh. Eksp. Teor. Fiz. **55**, 889 (1968) [JETP **28**, 461 (1969)].
- <sup>9</sup> P. Monceau, D. Saint-James, and G. Waysand, Phys. Rev. B **12**, 3673 (1975).
- <sup>10</sup> P. Mathieu, B. Plaçais, and Y. Simon, Phys. Rev. B **48**, 7376 (1993).
- <sup>11</sup> H. J. Fink, R. D. Kessinger, Phys. Rev. **140**, A1937 (1965).
- <sup>12</sup> L. N. Bulaevskii, M. Ledvij, and V. G. Kogan, Phys. Rev. B **46**, 366 (1992).
- <sup>13</sup> L. I. Glazman and A. E. Koshelev, Phys. Rev. B **43**, 2835 (1991).
- <sup>14</sup> A. V. Pan, R. Höhne, M. Ziese, P. Esquinazi, and C. Assmann, in *Physics and Materials Science of Vortex States, Flux Pinning and Dynamics*, NATO Science Series **356**, Kluwer A.P. (Dordrecht, 1999), p. 545.
- <sup>15</sup> A. V. Pan, *PhD thesis*, University of Leipzig (2000), unpublished.
- <sup>16</sup> M. G. Blamire, C. H. Marrows, N. A. Stelmashenko, and J. E. Evetts, Phys. Rev. B **67**, 014508 (2003).
- <sup>17</sup> A. V. Pan, R. Höhne, and P. Esquinazi, Physica B **329-333**, 1377 (2003).
- <sup>18</sup> I. Giaever, Phys. Rev. Lett. **15**, 825 (1965);
- <sup>19</sup> J. R. Clem, Phys. Rev. B **12**, 1742 (1975);
- <sup>20</sup> J. W. Ekin and J. R. Clem, Phys. Rev. B **12**, 1753 (1975).
- <sup>21</sup> P. Esquinazi, J. Low Temp. Phys. **85**, 139 (1991).
- <sup>22</sup> M. Ziese, P. Esquinazi and H. F. Braun, Superconductor Science and Technol. **7**, 869 (1994).
- <sup>23</sup> S. Knappe, C. Elster, and H. Koch, J. Vac. Sci. Technol. A **15**, 2158 (1997).
- <sup>24</sup> H. R. Hart and P. S. Swartz, Phys. Rev. **156**, 403 (1967).
- <sup>25</sup> H. J. Fink, L. J. Barnes, Phys. Rev. Lett. **15**, 792 (1965); P. S. Swartz, H. R. Hart, Phys. Rev. **156**, 412 (1967).
- <sup>26</sup> L. J. Barnes and H. J. Fink, Phys. Rev. **149**, 186 (1966); H. J. Fink and A.G. Presson, Phys. Rev. **151**, 219 (1966).
- <sup>27</sup> H. J. Fink, Phys. Rev. Lett. **21**, 853 (1965).
- <sup>28</sup> M. I. Tsindlekht and I. Felner, Physica B **329-333**, 1371 (2003).
- <sup>29</sup> A. E. Koshelev, P. H. Kes, Phys. Rev. B **48**, 6539 (1993).